MECSOL 2019 - Proceedings of the 7th International Symposium on Solid Mechanics
V. Tita, A. Ferreira, M.L. Ribeiro, A. Vieira and A.T. Beck (Editors), ABCM, Sao Carlos, SP, Brazil, April 15th to 17th, 2019

Cyclic Plasticity and Fatigue of 304L Stainless Steel under Proportional and Non-proportional Loading

C. Bemfica, E.N. Mamiya and F.C. Castro

Department of Mechanical Engineering, University of Brasilia, 70910-900 Brasilia, DF, Brazil

The cyclic plasticity and the fatigue behaviour of the 304L stainless steel were investigated at room temperature for fully-reversed strain-controlled axial, torsional, proportional axial-torsional and 90° out-of-phase non-proportional loading. Significant secondary hardening, associated with a martensitic phase transformation, was observed for axial and torsional loading, whilst mild or no secondary hardening occurred for proportional and non-proportional experiments. Measurable plastic strains were observed for all experiments, including those that did not fail after 2×10^6 cycles. The equivalent strain amplitude did not correlate the fatigue life for the investigated loading paths, whilst the Jiang fatigue model yielded life estimates within factor-of-four boundaries for most of the test data.
Keywords: stainless steel, plasticity, cyclic hardening, multiaxial fatigue, life prediction

INTRODUCTION

Grade 304 stainless steel is used in many industrial applications, like pressurized water nuclear reactors, aeronautical components and pressure vessels. This material exhibits a complex cyclic deformation behaviour, including several material phenomena that are not fully understood. Some of these phenomena are the secondary hardening (Baudry and Pineau, 1977; Bayerlein et al., 1989; Smaga et al., 2008), non-proportional hardening (Shamsaei and Fatemi, 2010), and ratcheting and creep (Taleb and Cailletaud, 2011; Taleb and Keller, 2017). The cyclic deformation behaviour is very important for fatigue analysis since several fatigue models are based upon stresses and strains. In this work, the cyclic deformation and the fatigue behaviour of the 304L stainless steel are investigated based upon axial, torsional, proportional axial-torsional and 90° out-of-phase experimental data, which are also used to evaluate the fatigue model proposed by Jiang (2000).

EXPERIMENTAL PROGRAMME

The 304L stainless steel was received as extruded bars, whose chemical composition in weight percentage is 0.018 C, 1.34 Mn, 0.034 P, 0.028 S, 0.43 Si, 18.16 Cr, 8.3 Ni, 0.22 Mo, 0.081 N, and Fe as balance. The bars were normalized at 1050 °C for 1h to eliminate dislocations structures and twins associated with the extrusion process. Afterwards, two types of specimens were machined: cylindrical solid (Fig. 1a) for axial loading, and thin-walled tubular specimens (Fig. 1b) for all other loading conditions. Specimens were grinded with sandpapers whose grit number ranged from 220 to 2500 to obtain a surface roughness less than 0.2 μm, following the ASTM E2207 Standard (ASTM, 2014).

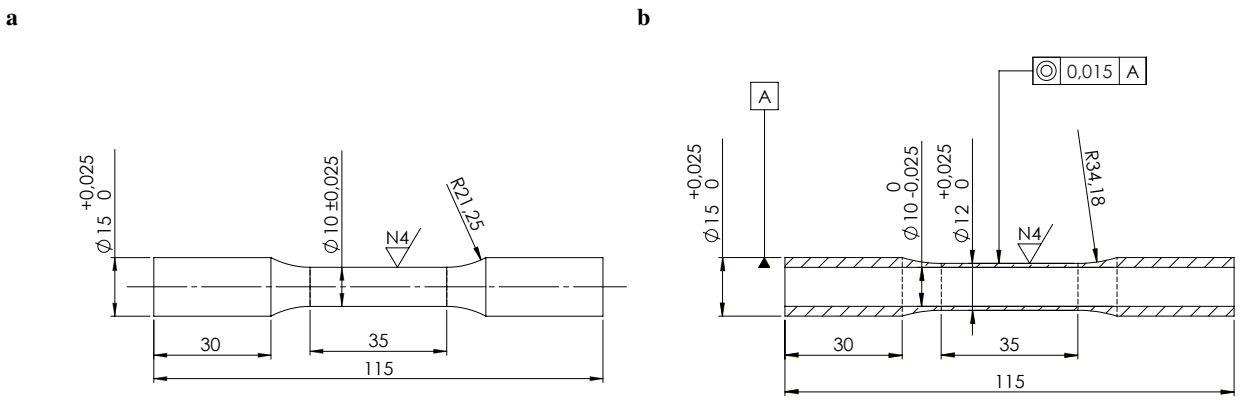

Figure 1 – Cylindrical solid (a) and thin-walled tubular (b) specimens. Dimensions in mm.

Experiments were performed by using an MTS 809 axial-torsional servo-hydraulic test system, whose capacity is ±100 kN and ±1100 N·m for axial force and torque, respectively. Axial and shear strains in the gauge section of the specimens were obtained by means of an MTS 632.80F-04 axial-torsional extensometer, whose axial strain and angle of twist ranges are -2.0–4.8% and -5–5°, respectively.

Four fully-reversed strain-controlled loading paths (Fig. 2) were investigated: axial, torsional, proportional axial-torsional and 90° out-of-phase non-proportional. Experiments were designed based upon the equivalent strain amplitude, $\Delta\varepsilon_{eq}/2$, defined as the radius of the minimum circle that circumscribes the strain path in the $\varepsilon - \gamma/\sqrt{3}$ space. The equivalent strain amplitude of proportional and non-proportional experiments preserved the ratio between axial and shear strain ranges $\Delta\gamma/\Delta\varepsilon$ of $\sqrt{3}$. Experiments were performed at room temperature and conducted until failure—defined as the appearance of a macroscopic fatigue crack, detected either by visual inspection or by a load drop of 5% of either force or torque—or run out—defined as 2×10^6 cycles.

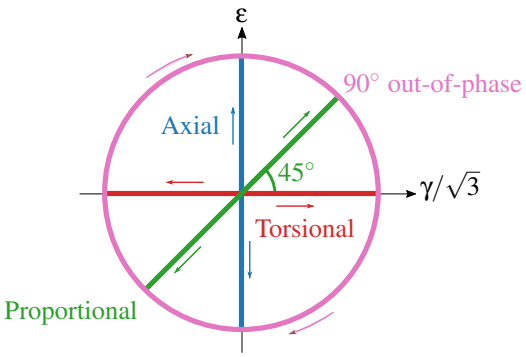

Figure 2 – Loading paths of fatigue experiments.

The 304L stainless steel exhibits a rate-dependent cyclic stress–strain behaviour (Krempl, 1979; Krempl and Lu, 1984), which was not the focus of this work. Hence, all experiments were carried out with an equivalent von Mises strain rate of approximately 10^{-2} s^{-1}. The only exception was the axial test whose $\Delta\varepsilon/2 = 0.20\%$, which was carried out with a higher strain rate to shorten the test duration. For this strain amplitude, Colin et al. (2010) did not observe a significant influence of strain rate upon the cyclic plasticity behaviour and fatigue life.

JIANG FATIGUE MODEL

Jiang (2000) proposed an incremental fatigue model that incorporates the concept of critical plane and plastic strain energy. The mathematical formulation of this model is

$$\mathrm{d}D = \left\langle \frac{\sigma_{mr}}{\sigma_0} - 1 \right\rangle^m \left(1 + \frac{\sigma}{\sigma_f}\right) \mathrm{d}Y, \tag{1}$$

in which

$$\mathrm{d}Y = b\sigma \mathrm{d}\varepsilon^p + \left(\frac{1-b}{2}\right) \tau \mathrm{d}\gamma^p. \tag{2}$$

In Eqs. (1) and (2) σ_{mr} is the memory stress—equals to the maximum von Mises equivalent stress for fully reversed loading—; σ_0 is the stress amplitude corresponding to the axial strain amplitude below which there is no fatigue failure; σ_f is the true fracture stress; $\sigma, \varepsilon^p, \tau$ and γ^p are respectively the normal stress, the normal plastic strain, the shear stress and the plastic shear strain at a given material plane; and m and b are material constants. $\langle x \rangle$ represents the Macaulay brackets. The fatigue cracking behaviour is determined by the material constant b, which can assume values between 0 (tensile mode) and 1 (shear mode). Failure occurs if cumulative fatigue damage reaches a critical value D_0, assumed to be a material constant. Mathematically,

$$D = \int \mathrm{d}D = D_0. \tag{3}$$

Note that a definition of a cycle, which is not straightforward for complex multiaxial loading, is not required for fatigue life

estimation. If fatigue damage per cycle is assumed to be constant, the predicted fatigue life can be calculated as

$$N_f = \frac{D_0}{\Delta D}, \tag{4}$$

in which ΔD is the fatigue damage associated with one loading cycle. For fully-reversed loading with minimal mean stress effect, ΔD can be calculated as

$$\Delta D = \left(\frac{\sigma_{mr}}{\sigma_0} - 1\right)^m \left[\oint b\sigma d\varepsilon^p + \oint \left(\frac{1-b}{2}\right)\tau d\gamma^p\right]. \tag{5}$$

Fatigue damage is calculated for all material planes, with different values for different material planes. The critical plane is assumed to be the material plane in which cumulative fatigue damage first reaches D_0.

RESULTS AND DISCUSSION

A summary of fatigue test data is shown in Tab. 1. It was investigated whether the equivalent strain amplitude, used to design fatigue experiments, could also predict fatigue lives. Based upon the results presented in Fig. 3, torsional experiments lasted longer than axial, which lasted longer than proportional, which lasted longer than 90° out-of-phase ones for the same equivalent strain amplitude. Therefore, this equivalent measure cannot predict the fatigue life of these loading paths.

Table 1 – Fatigue test data for the 304L stainless steel.

Loading Path	Specimen	$\Delta\varepsilon_{eq}/2$ [%]	$\Delta\varepsilon/2$ [%]	$\Delta\gamma/2$ [%]	$\Delta\sigma/2^*$ [MPa]	$\Delta\tau/2^*$ [MPa]	f [Hz]	N_f [Cycles]
Axial	UN14	1.00	1.00	–	451	–	0.15	643
	UN19	0.80	0.80	–	413	–	0.18	1,635
	UN06	0.50	0.50	–	253	–	0.50	4,218
	UN17	0.35	0.35	–	206	–	1.40	33,880
	UN24	0.28	0.28	–	200	–	2.00	88,900
	UN12	0.20	0.20	–	206	–	7.00	>1,901,074
Torsional	TU20	1.00	–	1.73	–	228	0.15	855
	TU29	1.00	–	1.73	–	267	0.15	1,800
	TU26	0.75	–	1.30	–	204	0.30	2,007
	TU21	0.50	–	0.87	–	186	0.50	18,230
	TU23	0.35	–	0.61	–	160	1.40	132,071
	TU28	0.28	–	0.48	–	182	2.00	>1,889,057
	TU22	0.20	–	0.35	–	132	2.00	>2,017,640
Proportional	TU40	1.00	0.71	1.22	304	128	0.30	461
	TU37	0.80	0.57	0.98	266	112	0.40	780
	TU33	0.60	0.42	0.73	235	99	0.60	830
	TU41	0.60	0.42	0.73	234	97	0.60	1,200
	TU32	0.50	0.35	0.61	209	90	0.80	2,000
	TU35	0.40	0.28	0.49	197	85	1.00	5,100
	TU36	0.30	0.21	0.37	186	80	1.20	35,000
	TU42	0.24	0.17	0.29	180	78	1.75	70,000
	TU38	0.20	0.14	0.24	156	74	2.00	148,700
90° out-of-phase	TU43	0.35	0.35	0.61	435	234	0.50	618
	TU44	0.30	0.30	0.53	397	211	0.60	1,200
	TU46	0.28	0.28	0.48	384	206	0.60	5,800
	TU45	0.25	0.25	0.43	349	187	0.70	9,700
	TU47	0.20	0.20	0.35	273	146	0.90	62,000

$\Delta\varepsilon_{eq}/2$, Equivalent strain amplitude; $\Delta\varepsilon/2$, Axial strain amplitude; $\Delta\gamma/2$, Shear strain amplitude; $\Delta\sigma/2$, Axial stress amplitude; $\Delta\tau/2$, Shear stress amplitude; f, Frequency; N_f, Number of cycles to failure.
* Half-life values.

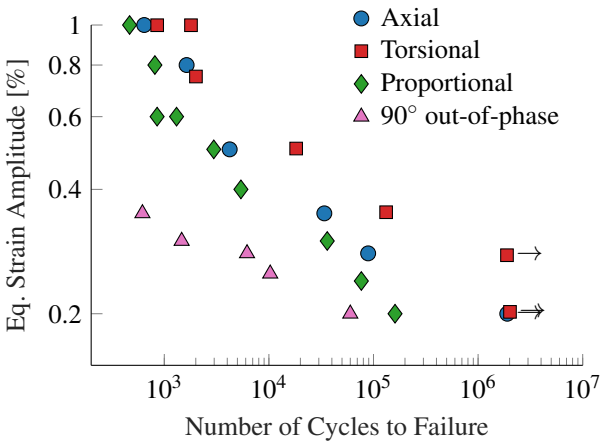

Figure 3 – Equivalent strain amplitude vs. fatigue life for the investigated loading paths.

The 304L stainless steel exhibits significant levels of plasticity even for low strain amplitudes. Hysteresis loops (Fig. 4) obtained after approximately 10^6 cycles for axial and torsional run-out tests feature plastic strain amplitudes of almost half the prescribed strain amplitude. This result suggests that the Jiang fatigue model—which predicts no fatigue damage if there is no plastic strain—can be used to predict the fatigue life even for low prescribed strain amplitudes. This may not apply for materials such as aluminium alloys, which may not exhibit measurable plastic strain for low strain amplitudes (Castro and Bemfica, 2018).

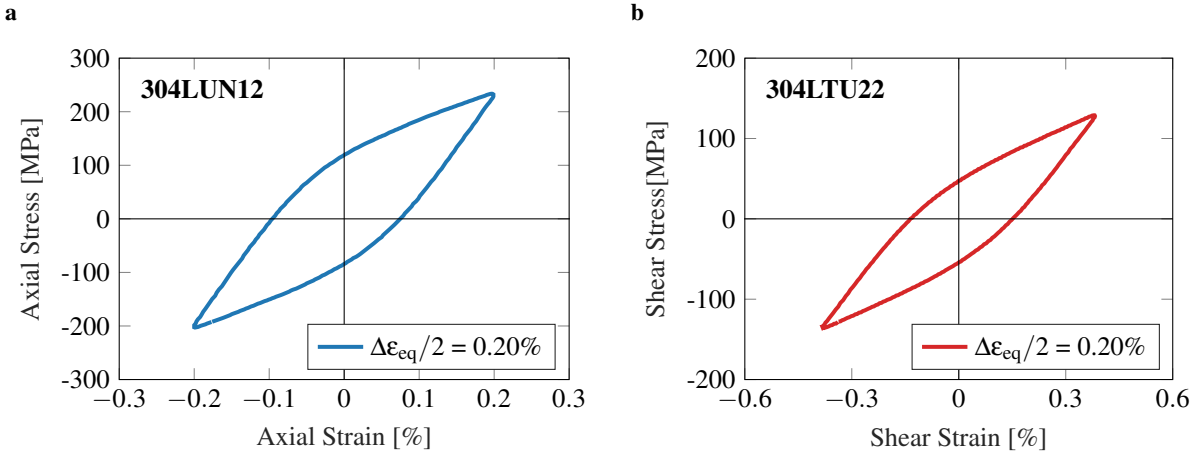

Figure 4 – Hysteresis loops for run-out axial (a) and torsional (b) tests.

The 304L stainless steel may not exhibit a stabilized cyclic stress–strain behaviour. For the same equivalent strain amplitude, the equivalent stress amplitude—defined as the radius of the minimum circle that circumscribes the deviatoric stress path (Jiang and Kurath, 1997)— varies throughout the loading cycles, as shown in Fig. 5. An early softening may be followed by a secondary hardening, associated with a martensitic phase transformation. Noticeable secondary hardening was observed for almost all axial and torsional experiments, including those in which specimens did not fail. Conversely, mild or no secondary hardening at all was observed for proportional and 90° out-of-phase experiments.

Due to the secondary hardening, it was investigated whether the usual fatigue analysis based upon the half-life cycle could be used to predict the fatigue life. Fatigue constants were obtained by fitting axial and torsional test data, with $b = 0.5$, $m = 1.49$, $\sigma_0 = 142$ MPa and $D_0 = 1.3 \times 10^7$. Fatigue life estimates are shown in Fig. 6, with the majority of life predictions within factor-of-four boundaries, represented by dotted lines. Life estimates for $N_f > 10^5$ cycles would probably improve if more axial and torsional experiments in this fatigue life regime were used to obtain fatigue constants. The half-life analysis is quite inexpensive from a computational point of view, in contrast with an incremental one. Furthermore, for an incremental analysis, it is not clear from which cycle material constants should be obtained since their values may be different depending upon the selected cycle. Therefore, this result suggests that this analysis is effective for estimating the fatigue life of the 304L stainless steel, at least for the investigated loading conditions.

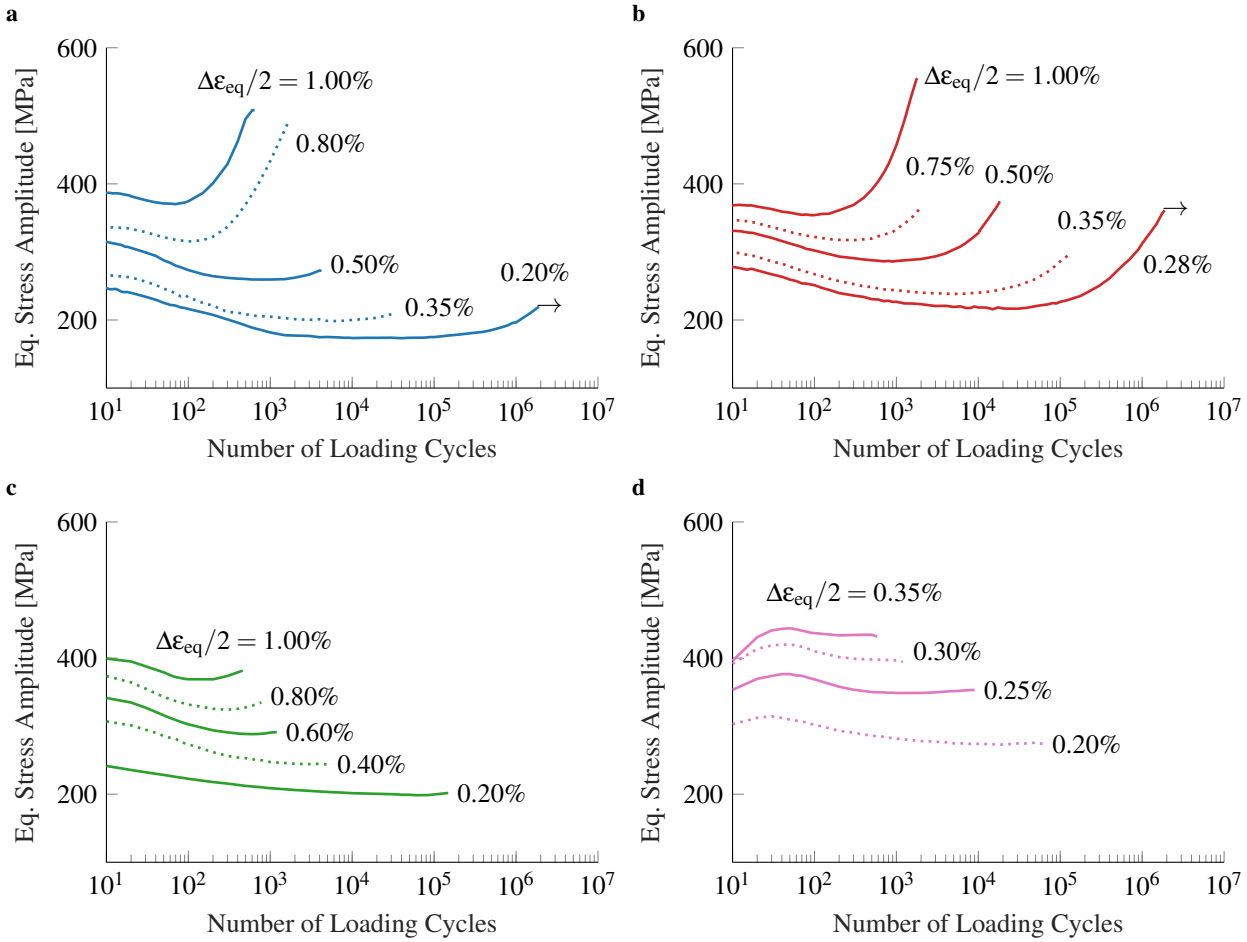

Figure 5 – Evolution of the equivalent stress amplitude for selected axial (a), torsional (b), proportional (c) and 90° out of phase (d) experiments.

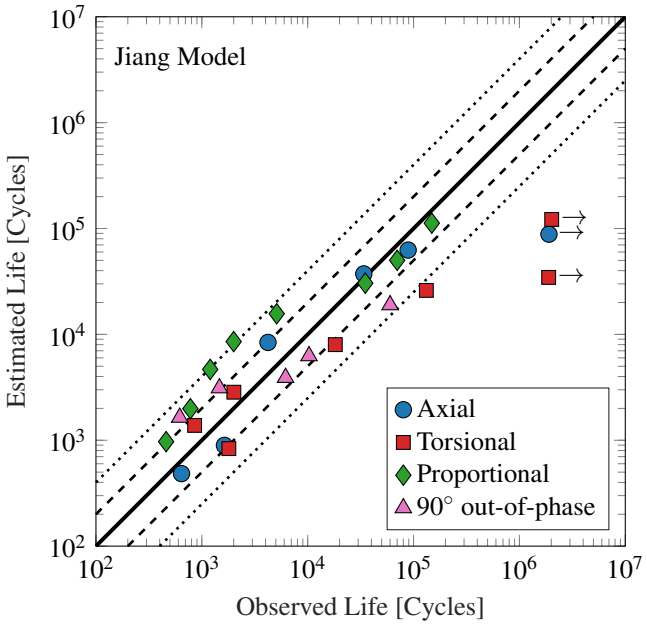

Figure 6 – Fatigue life estimates obtained from the Jiang fatigue model for half-life analysis.

CONCLUSIONS

The cyclic plasticity and the fatigue behaviour of the 304L stainless steel were investigated for fully-reversed strain-controlled axial, torsional, proportional axial-torsional and 90° out-of-phase non-proportional experiments at room temperature. Based upon the experimental results and the analysis presented in this work, the following conclusions can be drawn:

1. The equivalent strain amplitude cannot be used to predict the fatigue life for the investigated loading conditions.
2. Measurable plastic strains were observed for all prescribed equivalent strain amplitudes, including experiments that did not fail after 2×10^6 cycles.
3. Significant secondary hardening occurred for almost all axial and torsional tests, whilst proportional and non-proportional ones exhibited mild or no secondary hardening.
4. The Jiang fatigue model predicted the majority of fatigue lives within factor-of-four boundaries. Satisfactory life estimates were obtained from the usual fatigue analysis based upon the half-life stress–strain hysteresis loop, despite the occasional occurrence of secondary hardening.

ACKNOWLEDGEMENT

Fábio Castro and Edgar Mamiya would like to thank the support from CNPq (contracts 308126/2016-5 and 304083/2013-5). Cainã Bemfica acknowledges the support from CAPES (contract 1806204).

REFERENCES

American Society for Testing and Materials. ASTM E2207 - Standard Practice for Strain-Controlled Axial-Torsional Fatigue Testing with Thin-Walled Tubular Specimens, 2014.

G. Baudry and A. Pineau. Influence of strain-induced martensitic transformation on the low-cycle fatigue behaviour of stainless steel. Materials Science and Engineering, 28:229–242, 1977.

M. Bayerlein, H. J. Christ, and H. Mughrabi. Plasticity-induced martensitic transformation during cyclic deformation of AISI 304L stainless steel. Materials Science and Engineering A, 114(C):L11–L16, 1989.

F. Castro and C. Bemfica. Calibration and evaluation of the Lemaitre damage model using axial-torsion fatigue tests on five engineering alloys. Latin American Journal of Solids and Structures, 15(10):1–13, 2018

J. Colin, A. Fatemi, and S. Taheri. Fatigue Behavior of Stainless Steel 304L Including Strain Hardening, Prestraining, and Mean Stress Effects. Journal of Engineering Materials and Technology, 132(2):021008, 2010.

Y. Jiang. Fatigue criterion for general multiaxial loading. Fatigue and Fracture of Engineering Materials and Structures, 23(1):19–32, 2000.

Y. Jiang and P. Kurath. Nonproportional cyclic deformation: critical experiments and analytical modeling. International Journal of Plasticity, 13(8-9):743–763, 1997.

E. Krempl. An experimental study of room-temperature rate-sensitivity, creep and relaxation of AISI type 304 stainless steel. Mech. Phys. Solids, 27:363–375, 1979.

E. Krempl and H. Lu. Hardening and Rate-Dependent Behavior of Fully Annealed AISI Type 304 Stainless Steel Under Biaxial in-Phase and Out-of-Phase Strain Cycling At Room Temperature. Journal of Engineering Materials and Technology, Transactions of the ASME, 106(4):376–382, 1984.

N. Shamsaei and A. Fatemi. Effect of microstructure and hardness on non-proportional cyclic hardening coefficient and predictions. Materials Science and Engineering: A, 527(12):3015–3024, 2010.

M. Smaga, F. Walther, and D. Eifler. Deformation-induced martensitic transformation in metastable austenitic steels. Materials Science and Engineering A, 483-484(1-2 C):394–397, 2008.

L. Taleb and G. Cailletaud. Cyclic accumulation of the inelastic strain in the 304L SS under stress control at room temperature: Ratcheting or creep? International Journal of Plasticity, 27(12):1936–1958, 2011.

L. Taleb and C. Keller. Experimental contribution for better understanding of ratcheting in 304L SS. International Journal of Mechanical Sciences, (146-147): 527-53, 2018.

RESPONSIBILITY NOTICE

The authors are the only responsible for the printed material included in this paper.